Malaysian NANO-An International Journal

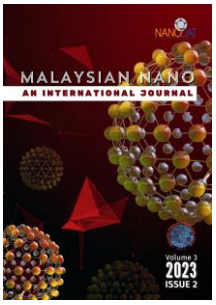

Research article

Gold nanoparticles supported on reduced graphene oxide as green catalyst for solventless hydrosilylation process

M. N. I. Amir[a], N. M. Julkapli[b], A. Ma'amor[a*]

[a]Department of Chemistry, Faculty of Science, Universiti Malaya, Kuala Lumpur 50603, Malaysia.
[b]Nanotechnology and Catalysis Research Centre (NANOCAT), Institute for Advanced Studies, Universiti Malaya, Kuala Lumpur 50603, Malaysia.

Received 17th August 2023
Revised 28th October 2023
Accepted 27th December 2023

DOI:
10.22452/mnij.vol3no2.2

Corresponding authors:
azman2111@um.edu.my

Abstract

The hydrosilylation reaction is a versatile process that is used to synthesize a variety of organosilicon compounds. However, the traditional metal oxide catalysts used for this reaction suffer from low activity and selectivity. This study focused on the synthesized and characterized gold nanoparticles (AuNPs)-reduced graphene oxide (rGO) catalyst for the hydrosilylation reaction. The AuNPs/rGO catalyst was synthesized by a one-pot method using trisodium citrate ($Na_3C_6H_5O_7$) as a reducing and capping agent. The catalyst was characterized by XRD, FESEM, and FTIR. The hydrosilylation reaction was carried out under solventless conditions using dimethylphenylsilane as the substrate. The AuNPs/rGO catalyst was found to be highly active and selective for the hydrosilylation reaction, yielding a 100% conversion of the substrate to disiloxane in 3 hours. The results of this study demonstrate the potential of AuNPs/rGO catalysts for the hydrosilylation reaction and suggest that they could be used to develop more efficient and sustainable processes for the synthesis of organosilicon compounds.

Keywords: gold nanoparticles; reduce graphene oxide; disiloxane; solventless; dehydrogenative coupling

1. Introduction

It is estimated that around 80% of industrial processes and many of the reactions of modern organic synthesis are catalytic processes [1-3]. Catalysts provide reaction mechanisms with adequate activation energies, making chemical transformation possible. Industrial catalysis is currently dominated by transition metals as active centers, which in general correspond to noble metals such as gold (Au) [4, 5], rhodium (Rh) [6, 7], iridium (Ir) [8], and platinum (Pt) [9, 10]. Other transition metals used are considered critical raw materials because they have very limited resources or are located in geographic areas subject to economic or political problems. Examples of these critical metals include ruthenium (Ru) [11], rhenium (Re) [12], osmium (Os) [13], tantalum (Ta) [14], and most rare earths. Gold nanoparticles (AuNPs) have been successfully applied in many organic reactions, such as hydrosilylation [15-17], cross-coupling [18-20], oxidation [21], and reduction [21, 22]. AuNPs have also been used as heterogeneous catalysts for the intermolecular hydroamination of terminal alkynes to afford amines under solventless conditions [21, 23]. The addition of graphene (G) to a platinum (Pt) catalyst can generate high electrocatalytic stability for the oxygen reduction reaction (ORR) in an acidic medium. The combination of Au and G in an electrocatalytic system has the potential to be further developed for possible applications as a cathodic ORR electrode in proton exchange membrane fuel cells [24]. The same is true for oxidation processes such as the conversion of ethylene to ethylene oxide, which is carried out in millions of tons per year and is based on the use of silver (Ag) [25, 26] and other metals. Recent research by Sawama, [27] has found that disiloxanes can be efficiently synthesized from hydrosilanes catalyzed by Au on carbon (C) using water as the oxidant at room temperature, resulting in the release of hydrogen gas. These processes are commonly used in organic synthesis, both on a laboratory scale and for the production of fine chemicals with applications in the pharmaceutical, phytosanitary, and electronics industries. They require the use of a common metal catalyst known as palladium (Pd) [28, 29]. With the research ambition to exploit the potential of G as a support for metal nanoparticles (MNPs), it is important and of interest to apply AuNPs supported on G as a catalyst in the aldehyde hydrosilylation process [30, 31]. It has been reported that AuNPs supported on oxide can efficiently act as heterogeneous catalysts for the reaction between hydrosilanes and alcohols, giving rise to the corresponding siloxane [31]. Considering these precedents, AuNPs supported on G is an obvious choice considering the known catalytic activity of Au in this reaction. Au catalysts have recently been intensively studied in relation to many important organic transformations and hydrogenation reactions, as Au's uniquely excellent selectivity towards the target product exceeds that of other

noble metals (Pd, Pt, or Ru), making it economically and environmentally attractive [32].

This study investigated the use of suitable catalysts for the hydrosilylation reaction to achieve high conversion rates and selectivity of products. The reaction time was also optimized to improve the activity of the catalysts. MNPs supported on G are superior to MNPs supported on other oxide supports because G modulates the electronic density on the MNPs, which can result in smaller MNPs and a stronger metal–support interaction that prevents metal leaching. The use of G as support is also expected to increase the reaction rates by bringing the substrates and reagents closer to the active MNPs. Cu and Pd nanoparticles (NPs) supported on G have been tested in the dehydrogenative coupling of alcohols with hydrosilanes and the dehydrogenative coupling of hydrosilanes with amines. For both processes, it was found that G is a very effective support that can lead to more efficient catalysts than MNPs deposited on other oxide supports. This research project is novel because no previous research has reported the use of AuNPs supported on graphene oxide (GO) for solventless hydrosilylation reactions with different molarities of AuNPs attached to the surface of reduced graphene oxide (rGO). AuNPs catalysts have recently been intensively studied in relation to many important organic transformations and hydrogenation reactions because Au's uniquely excellent selectivity towards the target product exceeds that of other noble metals (Pd, Pt, Ru), making it economically and environmentally attractive. AuNPs supported on a series of G materials were prepared using a one-pot method by adding Au^{2+} ions to a solution of varying molarity. The catalysts were then tested in the dehydrogenative coupling of hydrosilanes. The reaction conditions, such as residence time, catalyst loading, and type of Au-based catalyst, were optimized to find the best conditions for catalyst and reaction optimization. The reaction product, alkoxysilanes, is a highly valuable commodity reagent for surface coating.

2. Materials and Methods

Chloroauric acid ($HAuCl_4 \cdot 4H_2O$, ≥99%), trisodium citrate ($Na_3C_6H_5O_7$, ≥99%), benzaldehyde (C_7H_6O, ≥98%), toluene (C_7H_8, ≥99% GC), and n-dodecane ($CH_3(CH_2)_{10}CH_3$, ≥99% GC) were purchased from Nacalai Tesque. Dimethylphenylsilane ($C_8H_{12}Si$, ≥97%) was obtained from Tokyo Chemical Industry, and graphite powder (<20 μm) was purchased from Sigma Aldrich. All other chemicals were of analytical reagent grade and used as received, unless otherwise stated. Distilled water was used for all preparations. All reagents were used as received without further purification or modification, unless otherwise stated.

2.1 Synthesis GO

According to a previous report, GO was prepared using the improved Hummer's method [33]. Initially, graphite flakes (Sigma Aldrich, 20 μm) were oxidized using the same procedure with additional potassium permanganate ($KMnO_4$). For this method, a 9:1 mixture of concentrated sulfuric acid (H_2SO_4) and phosphoric acid (H_3PO_4) (360 mL: 45 mL) was added to a mixture of graphite flakes (3 g) and $KMnO_4$ (18 g), which was added slowly in portions to keep the reaction temperature below 20 °C. This produced a slight exotherm to 35-40 °C. The reaction was then heated to 50 °C and stirred for about 12 hours. The reaction mixture was immediately cooled to room temperature and poured onto ice (about 400 mL) together with 30% hydrogen peroxide (H_2O_2) (about 3 mL). For workup, the mixture was washed continuously with distilled (DI) water, 30% HCl, and ethanol. The mixture was centrifuged at 4000 rpm for 4 hours, and the initial step of washing was performed by centrifuging with 200 mL of DI water. The supernatant was then taken, while the residue/precipitate was decanted away. For the next washing, the residue or precipitate was taken, and the supernatant was decanted away. The remaining solid material (residue/precipitate) was then washed in succession with 200 mL of DI water, 200 mL of 30% HCl, and 200 mL of ethanol (2 times) for each wash. The solid material was stored in a cellulose bag and placed in a dialysis solution of DI water for 12 hours. The solids were obtained after the dialysis process and were oven-dried overnight at room temperature or using a freeze-drying process to obtain about 5 to 6 g of GO product.

2.2 Synthesis of AuNPs/rGO

AuNPs/rGO catalysts were synthesized by a one-pot reaction [34, 35, 36]. Initially, an aqueous solution of GO (0.275 mg/mL, 3 mL) was added to a solution of $HAuCl_4$ (0.047 mg/mL, 10 mL), and the mixture was aged for 30 minutes to promote the interaction of the Au^{3+} ions with the GO surfaces. The solution was then heated to 80 °C and a solution of trisodium citrate ($Na_3C_6H_5O_7$, about 0.085 $moldm^{-3}$, 188 mL) was added. Citrate is a reducing agent and capping agent that is commonly used in the environmentally friendly synthesis of AuNPs. It also reduces GO to rGO [34]. The mixture was kept at 80 °C with continuous stirring for 4 hours. The formation of AuNPs functionalized with rGO was indicated by the change in color of the solution from dark with a little yellow to a bluish purple. The solution was then cooled to room temperature, and the resulting solution was centrifuged (6000 rpm) and washed about three times with DI water to remove any free Au ions. The prepared catalyst was then dried through freeze-drying. The synthesis was repeated with different molar ratios of Au solution [36].

2.3 General Catalytic Procedure of Hydrosilylation Reaction

The corresponding catalyst of AuNPs/rGO (about 0.25 mol% of metal with respect to substrate) (about 5 mg) was introduced into a conical flask that had been refluxed by stirring. The aldehyde (9.4 mmol), which was benzaldehyde (about 1000 microliters), was added under ambient atmosphere and the AuNPs/rGO was sonicated together for about 30 minutes. Then, the hydrosilane (9.5 mmol), which was dimethylphenylsilane (1300 microliters), and dodecane (13 microliters), were added to the solution and the reactor was sealed properly for reflux reaction. The reaction mixture was magnetically stirred at 120 °C in an oil bath preheated at the reaction temperature. At the end of the reaction, the reaction mixture was cooled to room temperature and an aliquot of 0.1 mL was diluted with anhydrous toluene (0.5 mL), further diluted, and injected into GC-FID to determine the conversion and product yield based on the dodecane used as an internal standard [36].

The conversion rate of diphenyltetramethyldisiloxane (DTPMDS) with different molarities of AuNPs/rGO catalyst was calculated based on the analysis from GC-FID results. The calculation for the conversion rate of dimethylphenylsilane (DMPS) to DTPMDS is based on the method used in previous work [36].

2.4 Catalyst and Product Characterizations

The AuNPs/rGO catalysts were characterized using X-ray diffraction (XRD), scanning electron microscopy (SEM) with energy-dispersive X-ray spectroscopy (EDS), and Fourier transform infrared (FTIR) spectroscopy. The confirmation of catalytic performance and identification of final products were quantitatively and qualitatively analyzed using gas chromatography with flame-ionization detection (GC-FID) and mass spectrometry (GC-MS), respectively.

3. Results and discussion

3.1 Characterizations Analysis

XRD was used to investigate the morphology and structure of GO and the most optimized 0.4 mM AuNPs/rGO catalyst, based on the previous study [36] by identifying the d-spacing of cellular units. The diffractograms were identified according to the standard database of the International Centre for Diffraction Data (ICDD). The radiation with wavelength, λ of 1.54060 Å was used in the diffractometer. GO alone shows a peak exactly at $2\theta = 10°$, which has a d-spacing of 8.9 Å specific to the (011) plane (Figure 1). The smooth area observed 2θ values between 12 to 85 confirms the presence of rGO in the AuNPs/rGO, with the sample demonstrating both purity and effective prevention of rGO layer restacking by AuNPs [36].

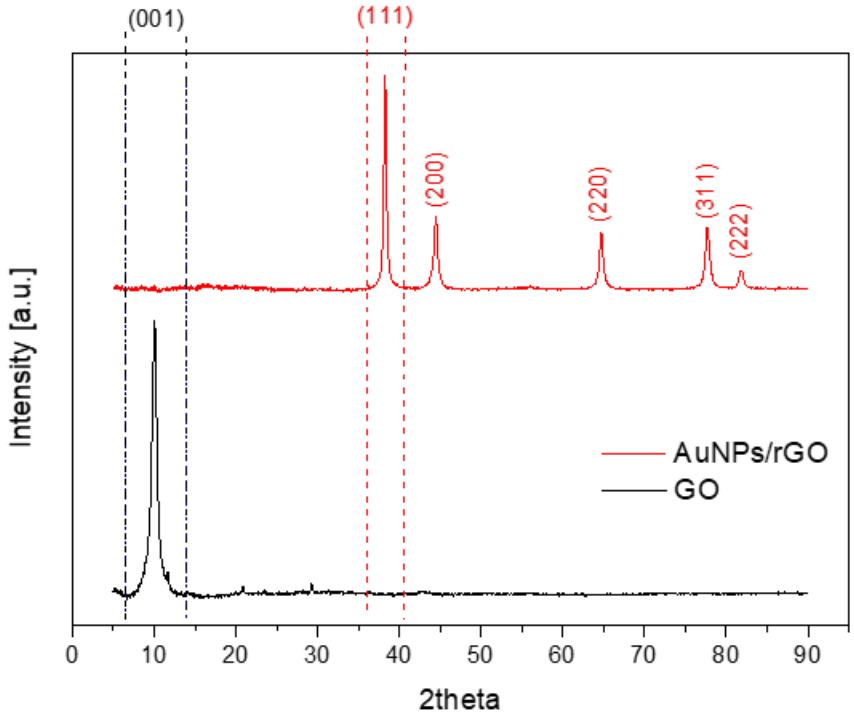

Figure 1: XRD pattern of AuNPs/rGO and GO.

It refers to molecular solids that have a repeated 3D pattern of atoms or molecules, identical in every portion [37]. This further verifies that the AuNPs/rGO catalyst was completely synthesized, as shown in the attached FESEM images for each different molarity of AuNPs/rGO samples (Figure 2). As seen in Figure 2, the Au crystallinity peaks decrease with the increasing Au composition in AuNPs/rGO. The surface images of the FESEM also show a clear difference in morphology, with an abundance of AuNPs visible at higher molarities compared to lower molarities of AuNPs/rGO. The small bright dots in the FESEM images in Figure 2 suggest the presence of AuNPs, which is further verified by the EDS analysis in Table 1 [38]. The number of bright dots increase proportionally with the Au composition in AuNPs/rGO. However, the Au crystallinity from the XRD diffractogram is disproportionate to the Au composition in EDS after 0.4 mM Au in optimized AuNPs/rGO [36].

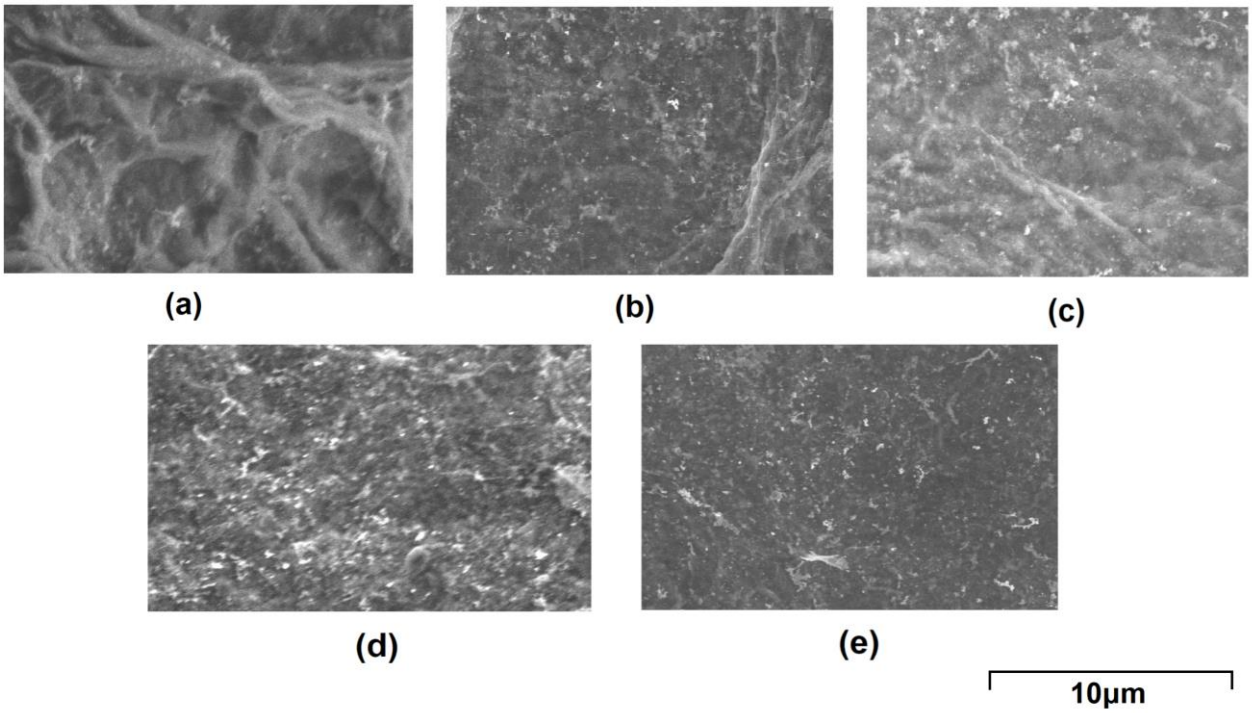

Figure 2: FESEM micrographs of AuNPs/rGO with different molarity of 0.2 mM (a), 0.4 mM (b), 0.6 mM (c), 0.8 mM (d), and 1.0 mM (eM).

Table 1 shows the wt % of AuNPs/rGO catalysts with different molarities from 0.2 to 1.0 mM. Figure 3 shows the EDS results for different precious metal loading of AuNPs on rGO, confirming the presence of Au, C, and O in the AuNPs/rGO catalyst.

Table 1: Amount of weight percent (%) for AuNPs/rGO catalyst with 1.0mM, 0.8 mM, 0.6 mM, 0.4 mM, and 0.2 mM

AuNPs/rGO catalyst (mM)	**Weight percent (wt %)**		
	C	O	Au
0.2	0.86	0.50	0.76
0.4	1.07	0.58	1.18
0.6	7.90	4.22	2.08
0.8	8.02	3.67	3.75
1.0	7.71	4.77	4.58

EDS analysis confirms the presence of nanoparticles in all 5 samples, as evidenced by the identification of the elements C, O, and Au. As expected, the EDS only shows 3 observable peaks for these 3 elements. The higher the Au content, the higher the diffraction angle of the EDS. For

example, the 1.0 mM AuNPs/GO catalyst has the highest weight percent (wt %) of 17.06 % (C: 7.71 %; O: 4.77 %; Au: 4.58 %), compared to the other AuNPs/rGO samples. This confirms that higher Au loading results in a higher diffraction angle [39].

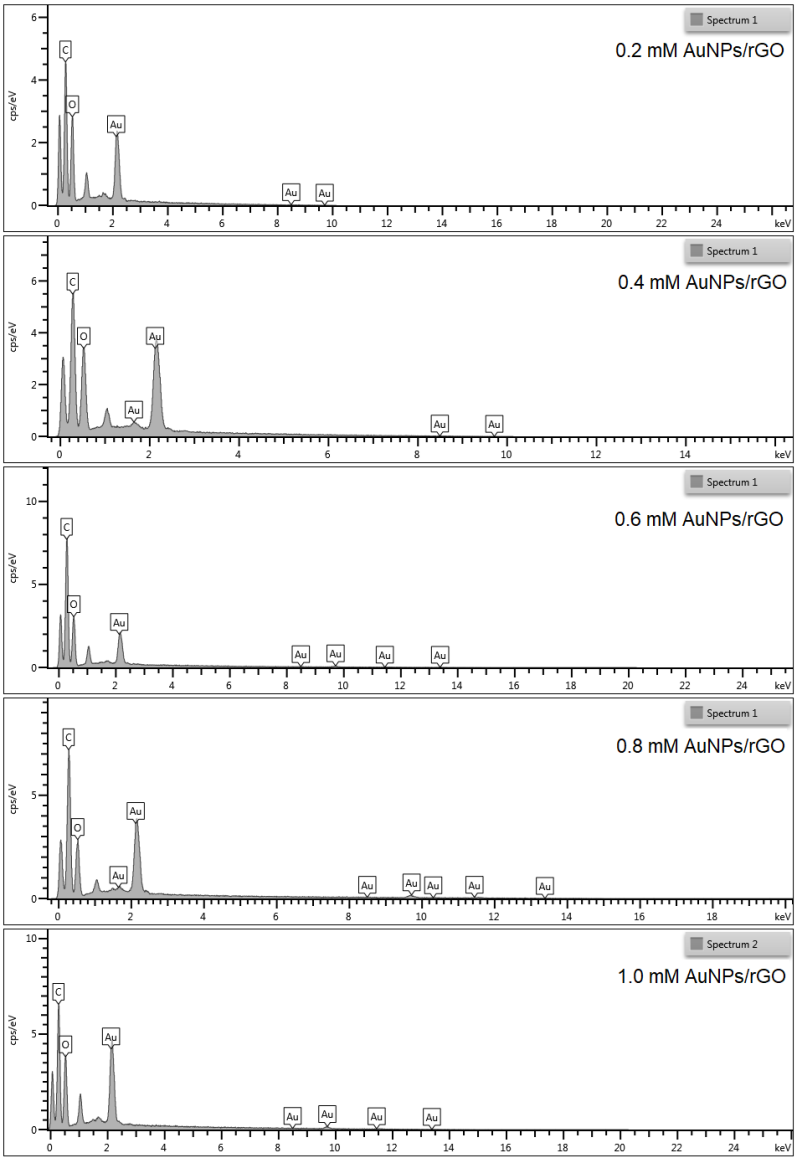

Figure 3: EDS image of AuNPs/rGO catalyst with 1.0mM, 0.8 mM, 0.6 mM, 0.4 mM, and 0.2 mM.

The functional groups on the surface of AuNPs were studied using FTIR analysis. The FTIR spectrum in Figure 4 (in the range of 500–4000 cm^{-1}) shows the spectra of 1.0 mM AuNPs/rGO, GO synthesized by freeze-drying, and graphite that was used to synthesize the GO. The reduction of GO was evident from the several peaks of C–O vibrations (1060 cm^{-1}) and C–OH stretching or O–H deformation of alcohol groups observed between 1273–1390 cm^{-1}. The peak of C=C stretches from unoxidized graphitic domains (1623 cm^{-1}), C=O (carboxyl group vibration – 1720 cm^{-1}), and C–H (aliphatic – 2805 cm^{-1}) are also present. Lastly, the obvious broad peaks of –OH

(hydroxyl) stretching bond vibrations or/and COOH functional groups can be seen at 3350 cm^{-1} [40]. In the case of the functionalized graphite and AuNPs/rGO, the intensity of these peaks decreased dramatically or even disappeared after synthesis and reduction, respectively. Conversely, the characteristic absorption peaks of –OH, –C=O in the AuNPs/rGO composite decreased dramatically, indicating the successful transformation from GO to rGO [41].

As seen in Figure 4 below, the peaks corresponding to the oxygen-containing functionalities of AuNPs/rGO were obviously decreased compared to the intensities of the GO peaks, and some even disappeared. This suggests that GO was reduced by trisodium citrate. However, not all peaks disappeared, which indicates that GO was not completely reduced by citrate as a reducing agent, thus indicating the presence of some functional groups [40].

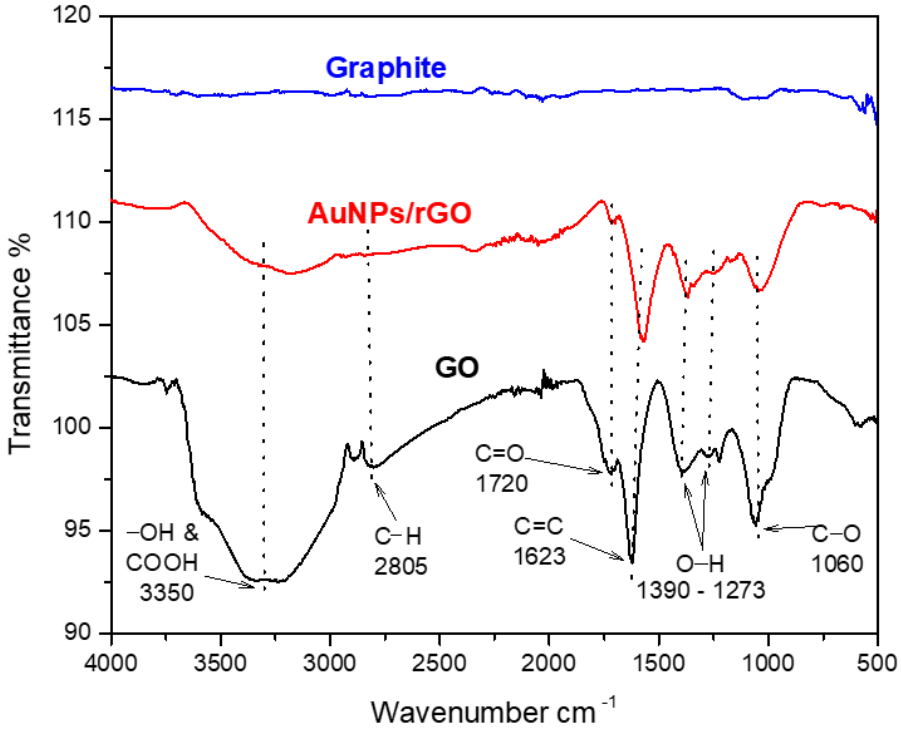

Figure 4: FTIR spectra of graphite, 1.0 mM of AuNPs/rGO and GO.

FTIR analysis confirmed the presence of citrate ligand on the surface of all AuNPs/rGO catalysts (Figure 5). The peak intensity of 1.0 mM AuNPs/rGO is the highest, and it decreases with the reduction of Au composition. GO was successfully reduced by trisodium citrate, as evidenced by the disappearance of the C=O stretching vibration peak at 1580 cm^{-1}. This is in line with the findings of Zhang and co-workers [34]. The carboxyl and -OH groups from trisodium citrate have formed strong hydrogen bonds with residual oxygen functionalities on the rGO surfaces, as seen by the peak at 3350 cm^{-1}. The surface-bound trisodium citrate can also be found at the intensity of the O–H deformation vibration peak at 1380 cm^{-1} (Figure 5). The trisodium

citrate vibrations are relatively small for 0.2 and 0.4 mM AuNPs/rGO, but the intensity increases at 0.6 and 0.8 mM AuNPs/rGO. The highest trisodium citrate vibrations are observed for 1.0 mM AuNPs/rGO. This shows that the citrate anionic ligand increases with the addition of Au composition in the catalyst. These findings confirm that trisodium citrate is strongly attached to the surface of rGO, as suggested by Zhang, Chen [34]. However, Tran, Nguyen [42] suggested that the citrate anionic ligand can possibly inhibit the active site of AuNPs. Therefore, these catalysts need to be tested in hydrosilylation reaction for a production of disiloxane to check the effect of citrate inhibition on catalyst surface.

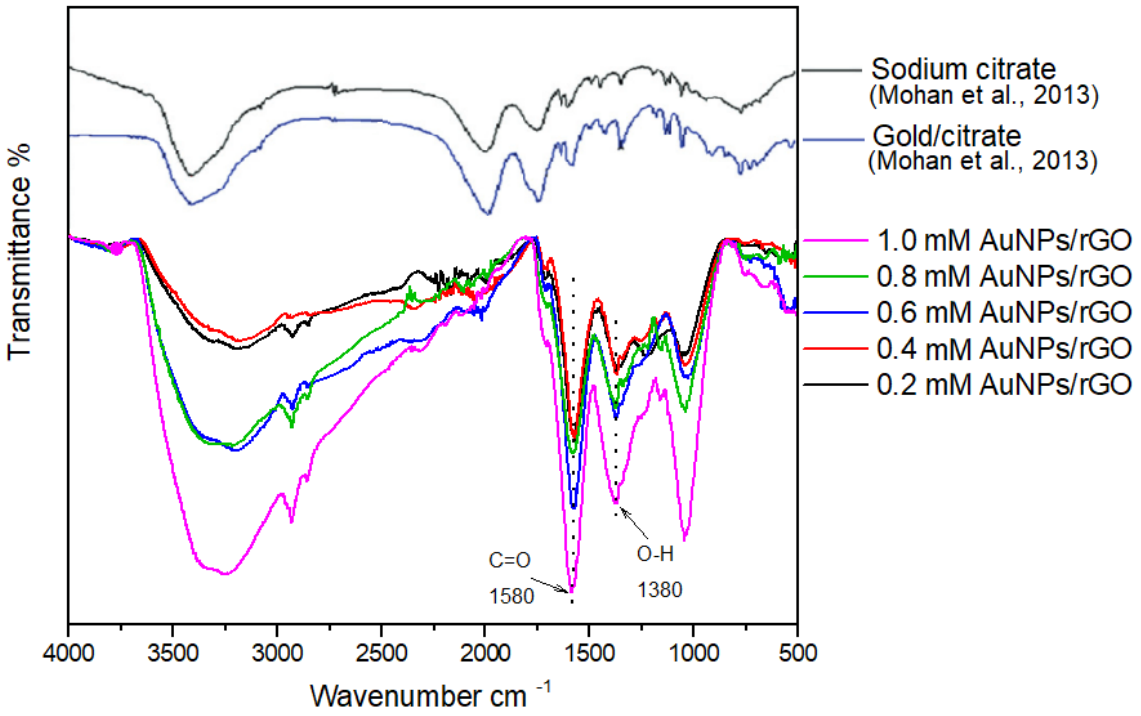

Figure 5: FTIR spectra of different molarity of AuNPs/rGO comparison together with spectra of sodium citrate and Au/citrate from Mohan, Praveen [43].

3.2 Disiloxane Production via Hydrosilylation Reaction

In the initial experiments, it was clearly observed that the dehydrogenative coupling of hydrosilane in a solventless reaction to produce disiloxane. The products were analyzed using different molarities of AuNPs/rGO catalyst. All the analyses showed an observable peak at around 26.3 minutes of retention time for GC-FID results, which confirmed the presence of organosiloxane of diphenyltetramethyldisiloxane (Figure 6). The product was further confirmed using GCMS analysis. The substrate was completely converted to product within 1 hour at 120 ˚C in benzaldehyde solvent.

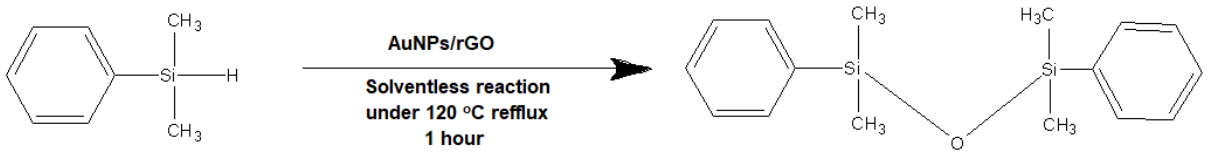

Figure 6: Dehydrogenative coupling of dimethylphenylsilane into diphenyltetramethyldisiloxane catalyzed AuNPs/rGO under solventless reaction at temperature of 120 °C within 1 hour.

The synthesis of disiloxane from organosiloxane or dehydrogenative coupling of dimethylphenylsilane was tested using AuNPs/rGO catalyst. As shown in Figure 7, the liquid solution turned from clear to yellowish transparent after the reaction was complete. The reaction was varied by analyzing different Au molar ratios attached to rGO, the reaction between solvent and solventless, and time.

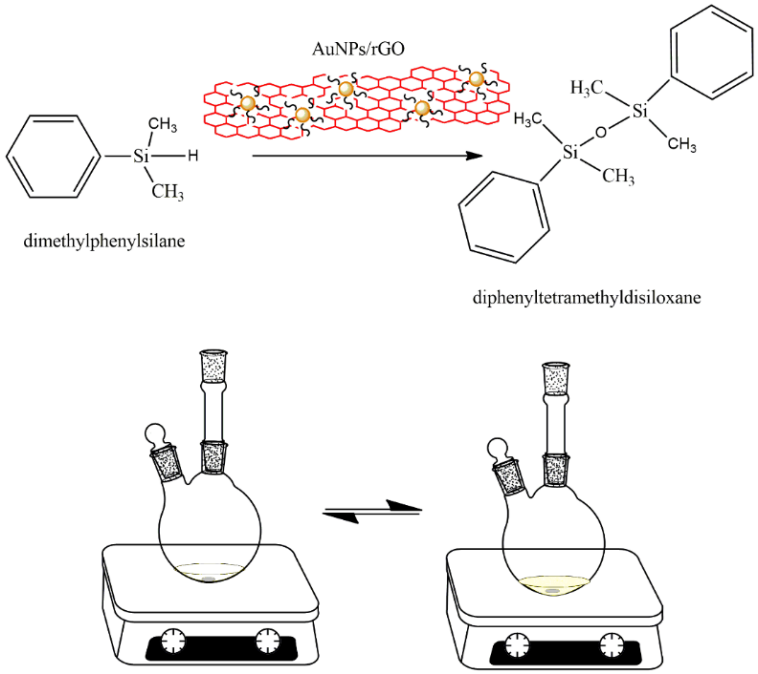

Figure 7: Schematic diagram of the reaction - dehydrogenative coupling of dimethylphenylsilane into diphenyltetramethyldisiloxane with AuNPs/rGO.

Table 2 shows the hydrosilylation reaction at 120 °C with different analyses using GO, an optimized sample of 0.4 mM AuNPs/rGO (solventless), and benzaldehyde as the solvent, all within one hour. This is supported in the previous study performed by Amir and co-workers [36]. While, no conversion was observed for the reaction using GO, as no catalyst's active component was present. From the reaction using 0.4 mM Au in AuNPs/rGO, it was found that the solventless reaction showed lower conversion, whereas the solvent reaction showed complete conversion in one hour using the same optimized catalyst. The highest product from this reaction was confirmed

with GCMS to be 1,3-diphenyltetramethyldisiloxane pure product after the reaction. It is worth mentioning that this reaction was a slow reaction due to the solventless reaction process. The reaction using solvent increased the diffusion of the feed to adsorb on the catalytic active site, thus increasing the reaction rate.

Table 2: The dehydrogenative coupling of dimethylphenylsilane with benzaldehyde into diphenyltetramethyldisiloxane catalysed by AuNPs/rGO

Hydrosilylation reaction	Conversion (%)
GO	0
Solventless	30
Solvent	100

Nevertheless, it is of interest to study hydrosilylation reaction in solventless conditions. Solventless reactions have many advantages, including low costs, simplicity of handling (especially important in industry), and reduced pollution [44]. To our knowledge, no study has been reported on hydrosilylation reactions catalyzed by AuNPs attached to rGO-based materials. Although solventless reactions show lower catalytic activity than solvent reactions (Table 2), this could be a major advantage for the chemical industry in the production of disiloxane, as the cost of the solvent is eliminated and the separation of the product from the solvent is unnecessary. Solventless reactions are also preferable when reactions proceed moderately in the absence of solvent or in an aqueous suspension [44, 45]. Therefore, solventless reactions could reduce the overall production cost of disiloxane.

The initial experiment was conducted to optimize the reaction conditions of solventless and time for the hydrosilanes. Only one product, 1,3-diphenyltetramethyldisiloxane, was observed based on GCMS analysis (Figure 8).

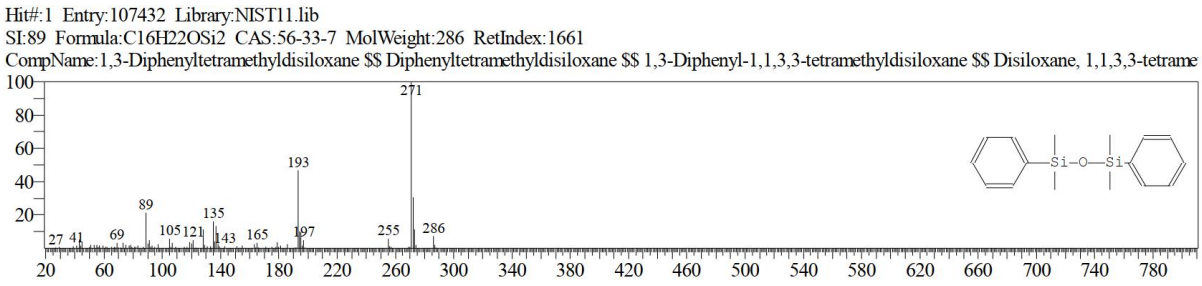

Figure 1: GC-MS spectrum of 1,3-diphenyltetramethyldisiloxane.

The compound 1,3-diphenyltetramethyldisiloxane (Figure 8) was synthesized by dehydrogenative coupling of dimethylphenylsilane catalyzed by AuNPs/rGO under solvent-free

conditions. The dehydrogenative coupling of dimethylphenylsilane into diphenyltetramethyldisiloxane was catalyzed by AuNPs/rGO using different concentrations of Au in the AuNPs catalyst series. The most optimized catalyst was found to be 0.4 mM AuNPs/rGO, which produced 28% conversion with 6.8 mmol of substrate remaining after 1 hour of reaction. The reactions with 0.6 and 0.8 mM AuNPs/rGO showed 10 and 8% conversion, respectively, while the catalyst with 1.0 mM Au showed the lowest catalytic activity at 2% conversion. The low hydrosilylation conversion was due to the deposition of citrate precursor at high Au concentrations of the catalyst, which led to catalyst deactivation. This finding agrees with Tran and co-workers [42], who showed that the presence of the citrate precursor inhibited AuNPs active sites.

FTIR analysis (Figure 5) showed that the concentrations of 0.2 mM and 0.4 mM Au in AuNPs/rGO showed small citrate vibrations, indicating that the citrate precursor did not inhibit AuNPs active sites. However, the citrate vibrations were significantly higher at Au concentrations from 0.6 to 1.0 mM, suggesting that the citrate precursor inhibited the AuNPs active sites, especially for the 1.0 mM AuNPs/rGO catalyst. Additionally, it was difficult for the reactant to adsorb onto the catalyst surface because the citrate precursor blocked the access, rendering AuNPs inactive.

4. Conclusions

Overall, GO-supported AuNPs were efficient catalysts for promoting the dehydrogenative coupling of dimethylphenylsilane by hydrosilylation reaction to produce disiloxane. The convenient variation of the molarity of Au salts over the GO surface caused the reduction process, while citrate was used as a reducing and capping agent simultaneously. GO was easily attached to AuNPs by a one-pot synthesis process, and the pure catalyst was obtained via freeze-drying. GO as a support exerts a noticeable influence on the catalytic activity of the optimized 0.4 mM AuNPs solution in a solventless reaction. Additionally, a comparison with other types of C media containing AuNPs indicates that GO properties were more suitable than other materials to support the development of catalysts that promote dehydrogenation coupling.

Conflicts of interest

The authors declare no conflict of interest.

Acknowledgements

This work was financially supported by Ministry of Higher Education Grant (FRGS/1/2017/STG01/UM/02/2) and University Malaya Research Grant (UMRG Programme) - AET (Innovative Technology (ITRC))–RP044B -17AET.

References

1. Okuhara, T., Water-tolerant solid acid catalysts. Chemical reviews, 2002. 102(10): p. 3641-3666.
2. Hattori, H., Solid base catalysts: generation of basic sites and application to organic synthesis. Applied Catalysis A: General, 2001. 222(1-2): p. 247-259.
3. Chiusoli, G.P. and P.M. Maitlis, Metal-catalysis in industrial organic processes. 2019: Royal Society of Chemistry.
4. Mashayekhi, N.A., M.C. Kung, and H.H. Kung, Selective oxidation of hydrocarbons on supported Au catalysts. Catalysis Today, 2014. 238: p. 74-79.
5. Zhang, S., et al., Recent advances of the combination of Au/acid catalysis. Chinese Journal of Chemistry, 2014. 32(10): p. 937-956.
6. Padwa, A., Rhodium (II) mediated cyclizations of diazo alkynyl ketones. Journal of Organometallic Chemistry, 2000. 610(1-2): p. 88-101.
7. Akutagawa, S., Asymmetric synthesis by metal BINAP catalysts. Applied Catalysis A: General, 1995. 128(2): p. 171-207.
8. Kim, S.B., Catalysis Application of Metal (Rh, Ir) Quinonoid Complexes. Journal of Inorganic and Organometallic Polymers and Materials, 2014. 24(1): p. 58-65.
9. Suchorski, Y. and W. Drachsel, Catalytic reactions on platinum nanofacets: bridging the size and complexity gap. Topics in Catalysis, 2007. 46(1): p. 201-215.
10. Blaser, H.-U., et al., Enantioselective hydrogenation of α-ketoesters using cinchona modified platinum catalysts and related systems: a review. Catalysis today, 1997. 37(4): p. 441-463.
11. Lohray, B. and V. Bhushan, in Enantioselective Catalysis. Organic Synthesis Highlights III, 1998. 3: p. 44.
12. Rueping, M. and B.J. Nachtsheim, A review of new developments in the Friedel–Crafts alkylation–From green chemistry to asymmetric catalysis. Beilstein Journal of Organic Chemistry, 2010. 6(1): p. 6.
13. Torrent, M., et al., Density functional study of the [2+ 2]-and [2+ 3]-cycloaddition

mechanisms for the osmium-catalyzed dihydroxylation of olefins. Organometallics, 1997. 16(1): p. 13-19.

14. Ishihara, A., et al., Tantalum oxide-based compounds as new non-noble cathodes for polymer electrolyte fuel cell. Electrochimica Acta, 2010. 55(26): p. 7581-7589.

15. Kidonakis, M. and M. Stratakis, Ligandless regioselective hydrosilylation of allenes catalyzed by gold nanoparticles. Organic letters, 2015. 17(18): p. 4538-4541.

16. Lantos, D., et al., Homogeneous gold-catalyzed hydrosilylation of aldehydes. Journal of organometallic chemistry, 2007. 692(9): p. 1799-1805.

17. Diez-Gonzalez, S. and S.P. Nolan, Copper, silver, and gold complexes in hydrosilylation reactions. Accounts of chemical research, 2008. 41(2): p. 349-358.

18. Nijamudheen, A. and A. Datta, Gold-Catalyzed Cross-Coupling Reactions: An Overview of Design Strategies, Mechanistic Studies, and Applications. Chemistry–A European Journal, 2020. 26(7): p. 1442-1487.

19. Liu, P. and J. Sun, Stereoselective Synthesis of Tetrasubstituted Furylalkenes via Gold-Catalyzed Cross-Coupling of Enynones with Diazo Compounds. Organic letters, 2017. 19(13): p. 3482-3485.

20. Garcia, P., et al., Gold-catalyzed cross-couplings: new opportunities for CC bond formation. ChemInform, 2010. 41(30): p. i.

21. Echavarren, A.M., A.S.K. Hashmi, and F.D. Toste, Gold catalysis–steadily increasing in importance. Advanced Synthesis & Catalysis, 2016. 358(9): p. 1347-1347.

22. Tomas-Mendivil, E., et al., Gold-Catalyzed Access to 1 H-Isochromenes: Reaction Development and Mechanistic Insight. ACS Catalysis, 2017. 7(1): p. 380-387.

23. Liang, S., et al., Commercial Supported Gold Nanoparticles Catalyzed Alkyne Hydroamination and Indole Synthesis. Advanced Synthesis & Catalysis, 2016. 358(20): p. 3313-3318.

24. Marinoiu, A., et al., Low-cost preparation method of well dispersed gold nanoparticles on reduced graphene oxide and electrocatalytic stability in PEM fuel cell. Arabian Journal of Chemistry, 2020. 13(1): p. 3585-3600.

25. Stegelmann, C., et al., Microkinetic modeling of ethylene oxidation over silver. Journal of Catalysis, 2004. 221(2): p. 630-649.

26. Goncharova, S., E. Paukshtis, and B. Bal'Zhinimaev, Size effects in ethylene oxidation on silver catalysts. Influence of support and Cs promoter. Applied Catalysis A: General, 1995. 126(1): p. 67-84.

27. Sawama, Y., et al., Disiloxane Synthesis Based on Silicon–Hydrogen Bond Activation using Gold and Platinum on Carbon in Water or Heavy Water. The Journal of Organic Chemistry, 2016. 81(10): p. 4190-4195.

28. Lyons, T.W. and M.S. Sanford, Palladium-catalyzed ligand-directed C− H functionalization reactions. Chemical reviews, 2010. 110(2): p. 1147-1169.

29. Littke, A.F. and G.C. Fu, Palladium-catalyzed coupling reactions of aryl chlorides. Angewandte Chemie International Edition, 2002. 41(22): p. 4176-4211.

30. Blandez, J.F., et al., Palladium nanoparticles supported on graphene as catalysts for the dehydrogenative coupling of hydrosilanes and amines. Catalysis Science & Technology, 2015. 5(4): p. 2167-2173.

31. Blandez, J.F., et al., Nickel nanoparticles supported on graphene as catalysts for aldehyde hydrosilylation. Journal of Molecular Catalysis A: Chemical, 2016. 412: p. 13-19.

32. Biradar, A.V. and T. Asefa, Nanosized gold-catalyzed selective oxidation of alkyl-substituted benzenes and n-alkanes. Applied Catalysis A: General, 2012. 435: p. 19-26.

33. Marcano, D.C., et al., Improved synthesis of graphene oxide. ACS nano, 2010. 4(8): p. 4806-4814.

34. Zhang, Z., et al., Sodium citrate: A universal reducing agent for reduction/decoration of graphene oxide with au nanoparticles. Nano Research, 2011. 4(6): p. 599-611.

35. Chuang, M.-K., et al., Gold nanoparticle-decorated graphene oxides for plasmonic-enhanced polymer photovoltaic devices. Nanoscale, 2014. 6(3): p. 1573-1579.

36 Amir, M.N.I., et al., Tuning lattice strain in Quasi-2D Au-rGO nanohybrid catalysts for dimethylphenylsilane solid state silylation to disiloxane. Materials Science and Engineering: B, 2023. 291: p. 116395

37. Krishnamurthy, S., et al., Yucca-derived synthesis of gold nanomaterial and their catalytic potential. Nanoscale research letters, 2014. 9(1): p. 627.

38. García, C.P., et al., Microscopic analysis of the interaction of gold nanoparticles with cells of the innate immune system. Scientific Reports, 2013. 3(1): p. 1-7.

39. Shang, L., et al., Graphene-supported ultrafine metal nanoparticles encapsulated by mesoporous silica: robust catalysts for oxidation and reduction reactions. Angewandte Chemie, 2014. 126(1): p. 254-258.

40. Emiru, T.F. and D.W. Ayele, Controlled synthesis, characterization and reduction of graphene oxide: A convenient method for large scale production. Egyptian Journal of Basic and Applied Sciences, 2017. 4(1): p. 74-79.

41. Amanulla, B., et al., Selective colorimetric detection of nitrite in water using chitosan stabilized gold nanoparticles decorated reduced graphene oxide. Scientific Reports, 2017. 7(1): p. 1-9.

42. Tran, T.D., et al., Gold nanoparticles as an outstanding catalyst for the hydrogen evolution reaction. Chemical Communications, 2018. 54(27): p. 3363-3366.

43. Mohan, J.C., et al., Functionalised gold nanoparticles for selective induction of in vitro apoptosis among human cancer cell lines. Journal of experimental nanoscience, 2013. 8(1): p. 32-4

44. Tanaka, K. and F. Toda, Solvent-Free Organic Reactions. Chem. Rev, 2000. 100: p. 1025-1074.

45. Loupy, A., Solvent-free reactions, in Modern Solvents in Organic Synthesis. 1999, Springer. p. 153-207.